Particle Accelerators
1984 Vol. 14 pp. 261-279
0031-2460/84/1403/0261$18.50/0

DYNAMICS OF A HIGH-CURRENT ELECTRON RING IN A CONVENTIONAL BETATRON ACCELERATOR

C. A. KAPETANAKOS, S. J. MARSH† and P. SPRANGLE

Advanced Accelerator Program, Naval Research Laboratory, Washington, D.C. 20375 U.S.A.

(Received July 5, 1983)

Analytical and computer-simulation results are reported on the dynamics of a high-current electron ring in a conventional betatron accelerator. These studies include, in addition to the external and self fields, the effects of surrounding walls and toroidal corrections.

Our results show that, in contrast with the modified betatron, the equilibrium in a conventional betatron is incompatible with either large thermal energy spread or emittance. However, as in the modified betatron, the energy mismatch and the diffusion of the self magnetic field impose stringent constraints on the accelerator. Finally, in both devices, it is necessary to keep the ratio of the beam minor radius to the torus minor radius much less than unity.

I. INTRODUCTION

Over the last few years, there is increasing interest on the development of ultra-high current accelerators. Currently, several laboratories[1–17] are engaged in studies that are aimed to assess the feasibility of developing such accelerators.

Induction acceleration, either in linear[1,2] or cyclic geometries,[3–17] is presently the most popular approach among the various accelerating schemes. Although the beam dynamics is relative simple in linear devices, their long length and high cost make them unattractive, when high energies are desired. For this reason, progressively more attention is focused on cyclic induction accelerators.

So far three different cyclic induction accelerators have been proposed: the conventional betatron,[18,19] the modified betatron,[4–16] and the stellatron.[17] The modified betatron includes in addition to the time-varying betatron magnetic field that is responsible for the acceleration, a strong toroidal magnetic field that substantially improves the stability of the conventional betatron. In the stellatron, the addition of a stellarator field to the modified betatron substantially reduces the displacement of the orbit that is due to energy mismatch. However, beam trapping and resonances appear to be major and presently unsolved problems.

The dynamics of a high-current electron ring confined in a modified-betatron configuration has been studied extensively over the last two years.[12–15] As a result of the finite v/γ of the electron ring, a host of new phenomena have either surfaced or become more pronounced. In this paper, we analyze and discuss the dynamics of a finite v/γ electron ring confined in a conventional betatron. The present work includes both analytical and computational studies for "cold" and "hot" electron rings. The results indicate that, in contrast with the modified betatron, the equilibrium in a

† Permanent Address: Sachs-Freeman Associates, Bowie, MD 20715 U.S.A.

conventional betatron is incompatible with either large thermal energy spread or emittance. In addition, it was found that for a "hot" ring, i.e., a ring with toroidal thermal energy spread, the radial ($\hat{\epsilon}_r$) component of the r.m.s. emittance oscillates in time, while the vertical component ($\hat{\epsilon}_z$) remains constant. Finally, the energy mismatch and the diffusion of the self magnetic field, as in the modified betatron, impose stringent constraints on the accelerator.

II. TRANSVERSE DYNAMICS

A. Macroscopic Beam Motion Without Toroidal Corrections

In this subsection, we study the dynamics of a high-current electron beam, including the effect of surrounding conducting walls. However, toroidal corrections associated with the fields are neglected. These corrections are considered in subsection C.

Consider a pencil-like electron beam inside a straight, perfectly conducting cylindrical pipe of circular cross section as shown in Fig. 1. The center of the beam is located at a distance Δr, Δz from the center of the minor cross section of the pipe. As a result of the induced charges on the wall, the center of the beam will experience a outward radial force, which for small displacements, i.e., Δr, $\Delta z \ll a$ is given by

$$\mathbf{F_E} = 2\pi e^2 n_0 (r_b/a)^2 \{\Delta r \hat{e}_r + \Delta z \hat{e}_z\}, \tag{1}$$

where a is the cylinder radius, r_b is the constant minor radius of the beam, and n_0 the uniform beam density.

Similarly, as a result of the induced current on the wall, the center of the beam will experience a radial force that is directed in the opposite direction from $\mathbf{F_E}$ and is given by

$$\mathbf{F_B} = -\beta_0{}^2 \mathbf{F_E}, \tag{2}$$

where $\beta_0 = v_{\theta 0}/c$ and $v_{\theta 0}$ is the beam speed in the toroidal direction.

In addition to the wall forces, the ring experiences the effect of the external fields, which are assumed to vary as

$$B_z(r, t) \cong B_{0z}(t)\{1 - n(r - r_0)/r_0\}, \tag{3a}$$

$$B_r(r, t) \cong -B_{0z}(t) nz/r_0, \tag{3b}$$

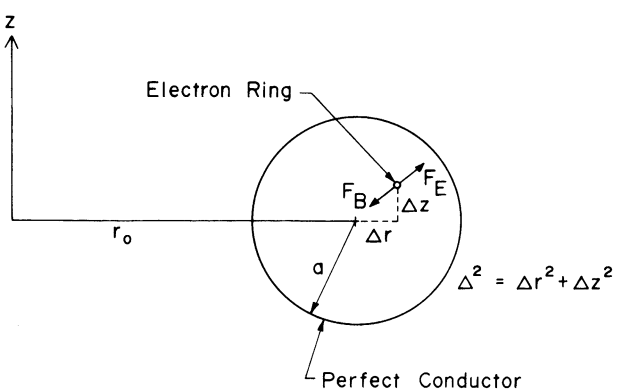

FIGURE 1 Wall (image) forces acting on a pencil-like beam, situated inside a perfectly conducting cylindrical pipe.

where r_0 is the major radius of the beam pipe and

$$E_\theta(r, t) = -\frac{1}{rc}\int_0^r r'\, dr' \frac{\partial B_z}{\partial t}(r', t). \tag{3c}$$

In the above equations $B_z(r, t)$ is the axial and $B_r(r, t)$ is the radial component of the betatron field, $E_\theta(r, t)$ is the induced electric field and n is the external-field index.

Using the induced fields of Eqs. (1) and (2), and the external field of Eqs. (3a) and (3b), the equations describing the temporal linear evolution of the beam's center, for time-independent applied fields, are

$$\Delta\ddot{r} + \tilde{\omega}_r^2\, \Delta r = \left(\frac{\Omega_{0z}}{\gamma_0}\right)\frac{\langle \delta P_\theta \rangle}{\gamma_0 m r_0}, \tag{4a}$$

and

$$\Delta\ddot{z} + \tilde{\omega}_z^2 \Delta z = 0, \tag{4b}$$

where

$$\tilde{\omega}_r^2 = (\Omega_{0z}/\gamma_0)^2\left(1 - n - n_s\frac{r_b^2}{a^2}\right), \quad \tilde{\omega}_z^2 = (\Omega_{0z}/\gamma_0)^2\left(n - n_s\frac{r_b^2}{a^2}\right), \tag{5}$$

$\Omega_{0z} = eB_{0z}/mc$, $n_s = 2(\nu/\gamma_0)(c/\Omega_{0z}r_b)^2$, ν is the Budker parameters, $\delta\gamma_0/\gamma_0 = \beta_0\langle \delta P_\theta \rangle/\gamma_0 m r_0 c$ and δP_θ is the difference between the canonical angular momentum of an electron at (r, z) and its corresponding value at the equilibrium orbit $(r_0, 0)$. The average is over initial coordinates and velocities. Equations (4) and (5) do not include the self electric and self magnetic fields, because both these fields are zero at the center of a straight beam.

In Eq. (4a), $\delta\gamma_0 = \beta_0\langle \delta P_\theta \rangle/m r_0 c$ indicates the energy mismatch, i.e., the difference between the energy of the reference electron (moving along the axis of the beam) and the energy required for the same electron to move on the equilibrium orbit $(r_0, 0)$. The solution of Eqs. (4) for time-independent fields is

$$\Delta r = \frac{\Omega_{0z}\langle \delta P_\theta \rangle}{\gamma_0^2 \tilde{\omega}_r^2 r_0 m} + \sum_j c_j e^{i\omega j t} + \text{c·c}, \tag{6}$$

and

$$\Delta z = \sum_j c_j e^{i\omega j t} + \text{c·c}, \tag{7}$$

where the c_j are constants and

$$\omega_j^2 = \begin{cases} \tilde{\omega}_r^2 \\ \tilde{\omega}_z^2 \end{cases}. \tag{8}$$

The first term on the RHS of Eq. (6) gives the displacement of the center of the orbit from the center of the surrounding cylindrical pipe and can be written as

$$\frac{\Delta r_0}{r_0} = \frac{\langle \delta P_\theta \rangle / \gamma_0}{(\Omega_{0z}/\gamma_0)(1 - n - n_s r_b^2/a^2) m r_0^2} = \frac{(\delta\gamma_0/\gamma_0)}{\beta_0^2(1 - n - n_s r_b^2/a^2)}. \tag{9}$$

The displacement of the orbit center because of the energy mismatch imposes very stringent constraints on the injector. This becomes apparent when we consider some limiting cases. For example, when $n = 1/2$ and $n_s r_b^2/a^2 \ll 1$, Eq. (9) is reduced to

$$\frac{\Delta r_0}{r_0} \approx 2(\delta\gamma_0/\gamma_0). \tag{10}$$

Equation (10) predicts that for a major radius $r_0 = 100$ cm, the ratio $\delta\gamma_0/\gamma_0$ should be less than 1% in order that the displacement of the orbit to be less than 2 cm. The condition $\delta\gamma_0/\gamma_0 \leqslant 1\%$ requires that the uncertainty in energy should be less than 35 keV when the energy of the injected beam is 3 MeV.

For the initial conditions $\Delta r = \Delta r(0)$ and $\Delta z(0) = \Delta\dot{r}(0) = \Delta\dot{z}(0) = 0$, Eqs. (6) and (7) give

$$\Delta r(t) = \Delta r_0 + (\Delta r(0) - \Delta r_0)\cos(\tilde{\omega}_r t), \tag{11a}$$

and

$$\Delta z(t) = 0, \tag{11b}$$

i.e., the center of the beam oscillates along the radial direction around Δr_0.

Equations (11) are in good agreement with the results of computer simulation shown in Fig. 2. The values of the various parameters are listed in Table I. The center of the ring perform sinusoidal oscillations around the equilibrium position that is located

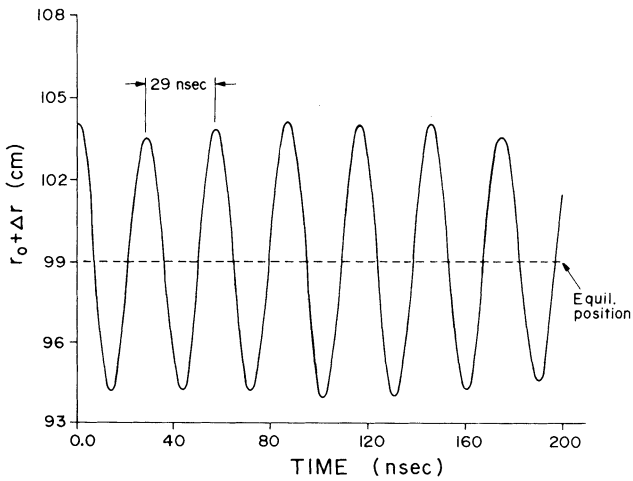

FIGURE 2 Radial oscillations around the equilibrium position performed by the center of the electron ring. The values of the various parameters for this computer run are listed in Table I.

TABLE I
Conventional Betatron Parameters

Run No. CONVBETA 0
Initial Beam Energy $\gamma_0 = 7.85$ (3.5 MeV)
Beam Current I (KA) = 5
Major Radius r_0 (cm) = 100
Initial Beam minor radius r_b (cm) = 8
Torus minor radius a (cm) = 16
Initial beam center position r_i (cm) = 104
Betatron Magn. Field at r_0, $z = 0$, B_{0z} (G) = 143.5
Initial emittance ϵ (rad − cm) = 0.400 (unnormalized)
Initial temperature spread (half width) $\Delta\gamma/\gamma_0 = 0.0$
External-field index $n = 0.447$
Self-field index $n_s = 0.16$

99 cm from the major axis ($\Delta r_0 = -1$ cm) with a frequency $\tilde{\omega}_r$ given by Eq. (5), which gives a period of about 28 nsec, in agreement with the computer results. Such a pure radial motion cannot occur in a modified betatron configuration, because the toroidal magnetic field couples the r and z motions.

The orbit of the beam's center is not always a straight line. For example, when $\Delta r(0)$ and $\Delta\dot{z}(0) \neq 0$ but $\Delta\dot{r}(0) = \Delta z(0) = 0$

$$\Delta r = \Delta r_0 + \left(\Delta r(0) - \Delta r_0\right) \cos \tilde{\omega}_r t,$$

and

$$\Delta z = \left(\frac{\Delta\dot{z}(0)}{\tilde{\omega}_z}\right) \sin \tilde{\omega}_z t,$$

which for $\tilde{\omega}_r = \tilde{\omega}_z$ gives an ellipse as shown in Fig. 3.

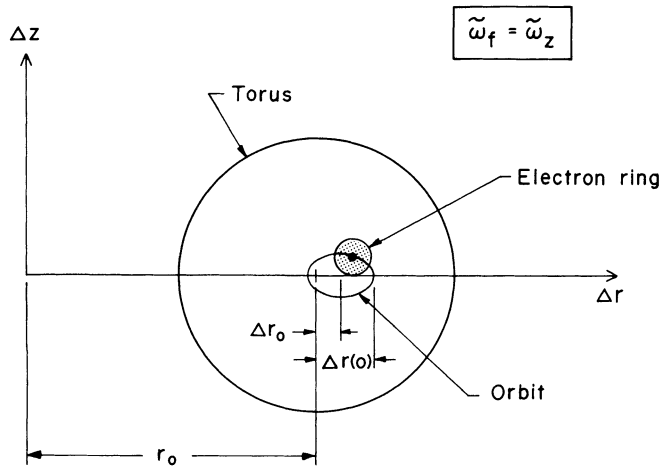

FIGURE 3 Under appropriate initial conditions, the center of the ring can describe an ellipse.

The linearized Eqs. (1) and (2) are based on the assumption that $\Delta r/a$ and $\Delta z/a \ll 1$. If this assumption is not satisfied, it is shown in Appendix A that for an arbitrary minor radius beam of uniform charge and current density, the fields at the center of the straight beam are given by

$$E_\rho(\Delta) = -\frac{2|e|N_l}{a^2}\frac{\Delta}{(1-\Delta^2/a^2)}, \tag{12a}$$

and

$$B_\phi(\Delta) = -\frac{2|e|N_l\beta_0}{a^2}\frac{\Delta}{(1-\Delta^2/a^2)} = -\frac{2|e|N_l\beta_0}{a}\sum_{l=1}^{\infty}\left(\frac{\Delta}{a}\right)^{2l-1}, \tag{12b}$$

provided that the beam does not touch the perfectly conducting wall. In Eqs. (12), $\Delta^2 = \Delta r^2 + \Delta z^2$, N_l is the number of electrons per unit length in the beam.

Since for a completely non-neutral beam the electric field force is greater than the magnetic force, the beam density does not remain uniform whenever a section of the beam is near a conducting wall, but rather develops a peak at its outer edge facing the wall.

As a consequence of the beam-density profile distortion, the ratio Δ/a increases, leading to larger-amplitude oscillation that could result in substantial particle losses, as shown in Fig. 4. In this run, at $t = 0$ the surface of the beam is more than 1 cm away from the wall and the beam center was arranged to move toward the equilibrium position. However, the wall forces reversed the direction of motion and most of the beam was lost in a short period of time. Therefore, in order to avoid the nonlinearities of image forces, it is necessary to keep the electrons far away from the wall. Typically, the ratio $(\Delta + r_b)/a \leqslant 0.5$, where r_b is the beam radius.

B. Individual Particle Motion

In the system of coordinates shown in Fig. 5, the equations describing the motion of individual electrons in a constant-radius beam are

$$\delta\ddot{r} + \hat{\omega}_r^2\,\delta r = \frac{c^2}{r_0}\frac{\Delta\gamma}{\gamma_0}, \tag{13a}$$

and

$$\delta\ddot{z} + \hat{\omega}_z^2\,\delta z = 0, \tag{13b}$$

where $\hat{\omega}_r^2 = (\Omega_{0z}/\gamma_0)^2(1 - n - n_s)$, $\hat{\omega}_z^2 = (\Omega_{0z}/\gamma_0)^2(n - n_s)$, and $\Delta\gamma = \gamma - \langle\gamma\rangle = (v_{\theta 0}\gamma_0^3/c^2)(v_\theta - \langle v_\theta\rangle)$ i.e., the toroidal energy spread in the beam.

For time-independent fields, the solution of Eqs. (13) is

$$\delta r = \delta r_0 + [\delta r(0) - \delta r_0]\cos\hat{\omega}_r t + \frac{\delta\dot{r}(0)}{\hat{\omega}_r}\sin\hat{\omega}_r t, \tag{14a}$$

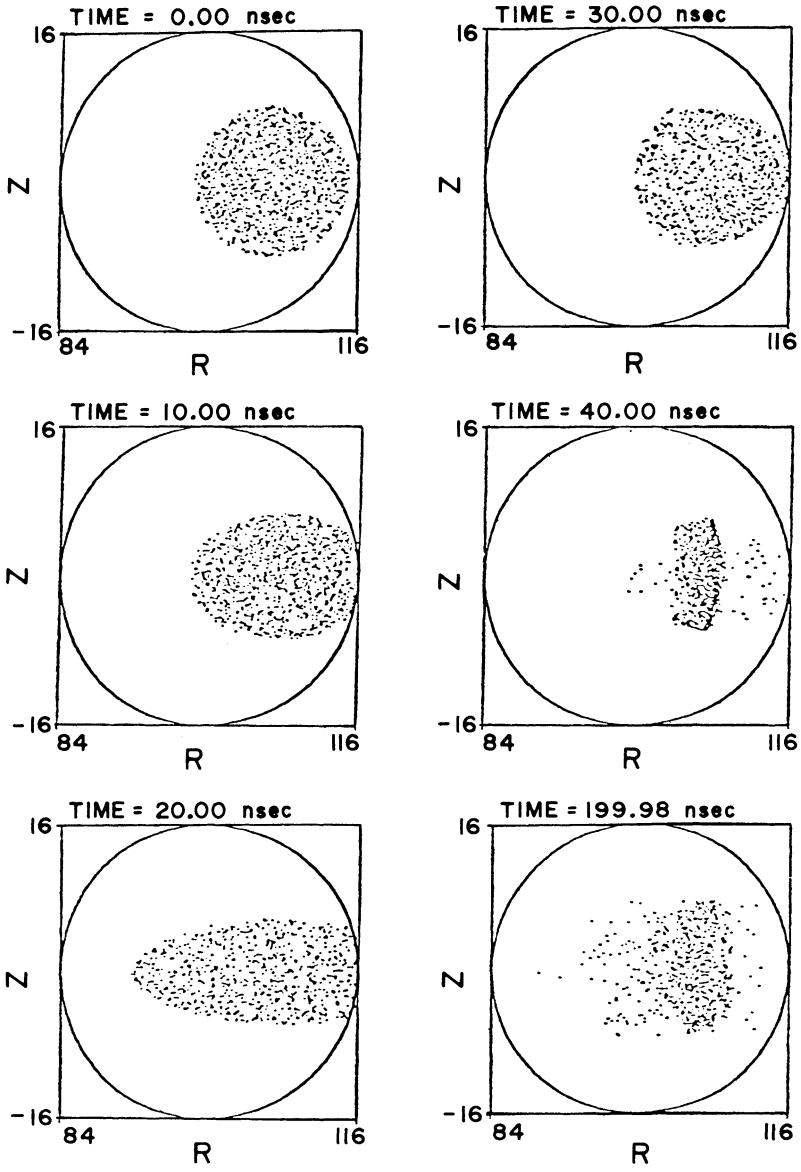

FIGURE 4 Snap-shots of the electron ring minor cross section. The nonlinear image forces can have a detrimental effect on the beam when the beam surface is very near the wall. The various parameters for this computer run are listed in Table II.

and

$$\delta z = \delta z(0) \cos \hat{\omega}_z t = \frac{\delta \dot{z}(0)}{\hat{\omega}_z} \sin \hat{\omega}_z t, \tag{14b}$$

where $\delta r_0 = (c^2/r_0 \omega_r^2)(\Delta\gamma/\gamma_0)$ and $\delta r(0)$, $\delta z(0)$, $\delta \dot{r}(0)$, $\delta \dot{z}(0)$ are the initial position and velocity components of the particle.

TABLE II

Conventional Betatron

Run No. CONVBETA 08
Initial Beam Energy $\gamma_0 = 7.85$ (3.5 MeV)
Beam Current I (KA) = 5
Major Radius r_0 (cm) = 100
Initial Beam minor radius r_b (cm) = 8
Torus minor radius a (cm) = 16
Initial beam center position r_i (cm) = 107
Betatron Magn. Field at r_0, $z = 0$, B_{0z} (G) = 136.1
Initial emittance ϵ (rad − cm) = 0.200 (unnormalized)
Initial temperature spread (half width) $\Delta\gamma/\gamma = 0$
External-field index $n = 0.447$
Self-field index $n_s = 0.18$

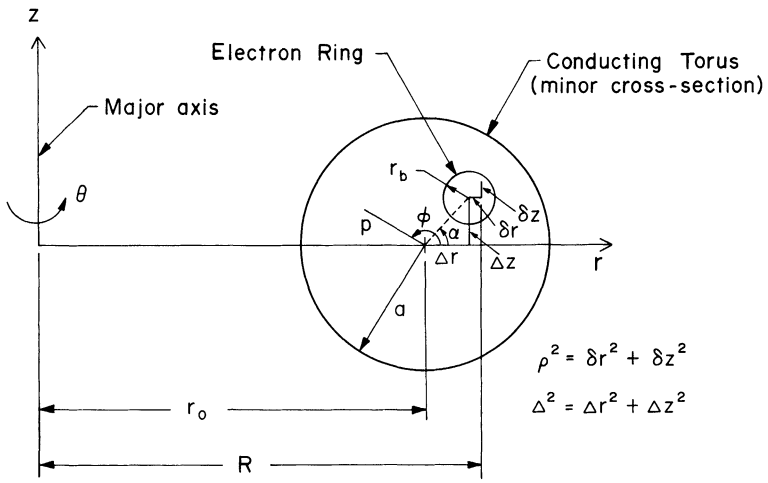

FIGURE 5 System of coordinates for Eq. (13).

For $n = 1/2$, the two frequencies are equal, i.e., $\hat{\omega}_r = \hat{\omega}_z = \omega$ and the r.m.s. beam emittances become

$$\hat{\epsilon}_r^2 = \frac{16}{v_{\theta 0}^2}\{\langle \delta r^2(t)\rangle\langle \delta \dot{r}^2(t)\rangle - \langle \delta r(t)\,\delta \dot{r}(t)\rangle^2\}$$

$$= \frac{16}{v_{\theta 0}^2}\{\langle \delta r^2(0)\rangle\langle \delta \dot{r}^2(0)\rangle + \langle \delta r_0^2\rangle[\omega^2\langle \delta r^2(0)\rangle \sin^2 \omega t + \langle \delta \dot{r}^2(0)\rangle(\cos \omega t - 1)^2]\}, \tag{15a}$$

and

$$\hat{\epsilon}_z^2 = \frac{16}{v_{\theta 0}^2}\{\langle \delta z^2(0)\rangle\langle \delta \dot{z}^2(0)\rangle\}. \tag{15b}$$

Equations (15) are based on the assumption that at $t = 0$ the beam is in a KV distribution[20] and thus

$$\langle \delta r(0) \rangle = \langle \delta \dot{r}(0) \rangle = \langle \delta r_0 \, \delta r(0) \rangle = \langle \delta r(0) \, \delta \dot{r}(0) \rangle$$
$$= \langle \delta z(0) \rangle = \langle \delta \dot{z}(0) \rangle = \langle \delta z(0) \, \delta \dot{z}(0) \rangle = 0.$$

In addition, for such a distribution, it is easy to show that

$$\langle \delta r^2(0) \rangle = \langle \delta z^2(0) \rangle = r_b^2/4, \tag{16}$$

and

$$\langle \delta \dot{r}^2(0) \rangle = \langle \delta \dot{z}^2(0) \rangle = v_\perp^2(0)/4 \simeq \frac{\omega^2 r_b^2}{4}. \tag{17}$$

Substituting Eqs. (16) and (17) into Eqs. (15), we obtain

$$\hat{\epsilon}_r^2 = \epsilon^2 \left[1 + \frac{8\langle \delta r_0^2 \rangle}{r_b^2} (1 - \cos \omega t) \right], \tag{18a}$$

and

$$\hat{\epsilon}_z^2 = \epsilon^2, \tag{18b}$$

where

$$\epsilon = r_b v_\perp(0)/v_{\theta 0}, \tag{19}$$

and

$$\omega^2 = (\Omega_{0z}/\gamma_0)^2(1 - n - n_s). \tag{20}$$

Intense electron rings with thermal energy spread have been simulated numerically. For the run shown in Fig. 6, the various parameters are listed in Table III. Figures 6a, 6b and 6c give the variation of γ with radial distance, the configuration space and the phase spaces for three different times. It is observed that the ring envelope varies sinusoidally with a peak radial amplitude that is almost twice of its initial value. This is consistent with Eq. (14a), which predicts that thermal effects will increase the radial excursions of the electrons by $2\Delta r_0$. For $r_0 = 100$ cm, $n = 0.45$, $n_s = 0.29$ and a fractional thermal half width $\delta = 1\%$, the additional radial excursion will be $2\Delta r_0 = 2r_0 \, \delta/(1 - n - n_s) = 8$ cm, i.e., equal to the initial beam radius. In constrast, in a high-current modified betatron, n_s can be considerably greater than unity and thus the radial excursions can be substantially smaller.[12]

The variation of the r.m.s. emittance as a function of time is shown in Fig. 6d. In accordance with Eq. (18b), $\hat{\epsilon}_z$ remains approximately constant in time. However, $\hat{\epsilon}_r$ oscillates with a period that is about 38 nsec. For the parameters of the present run, Eq. (20) predicts a period of about 40 nsec. The small difference is probably related to toroidal effects. In addition to the period, the shape of the oscillations predicted by Eq. (18a) is very similar to that of Fig. 6d. Moreover, Eq. (18a) predicts a peak

(a)

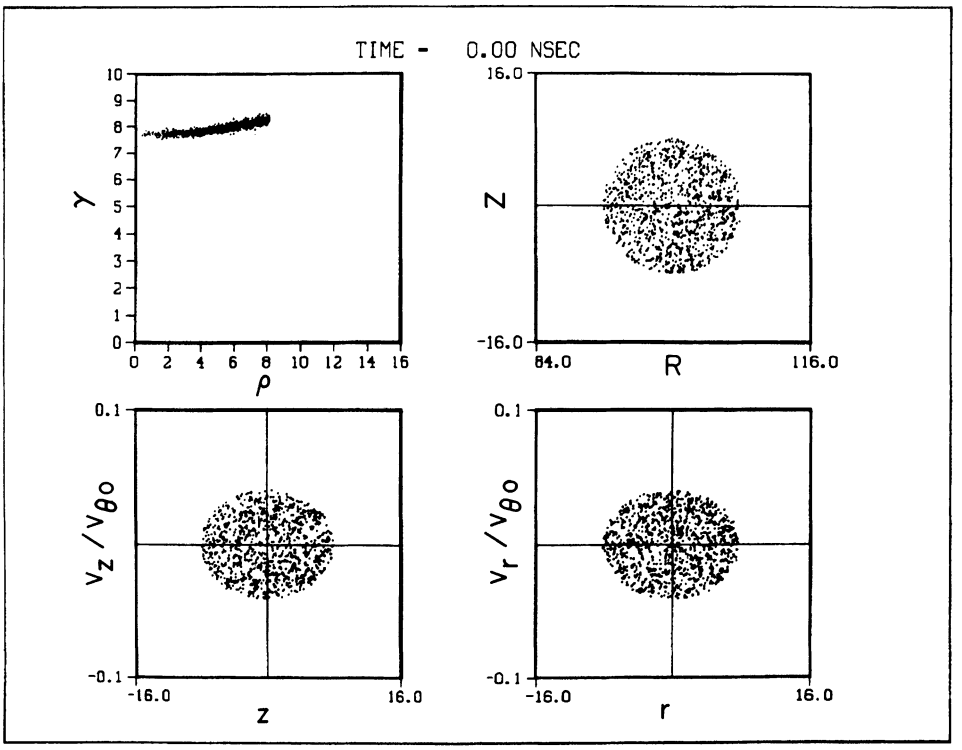
TIME - 0.00 NSEC
γ
ρ
Z
R
$v_z / v_{\theta o}$
z
$v_r / v_{\theta o}$
r

(b)

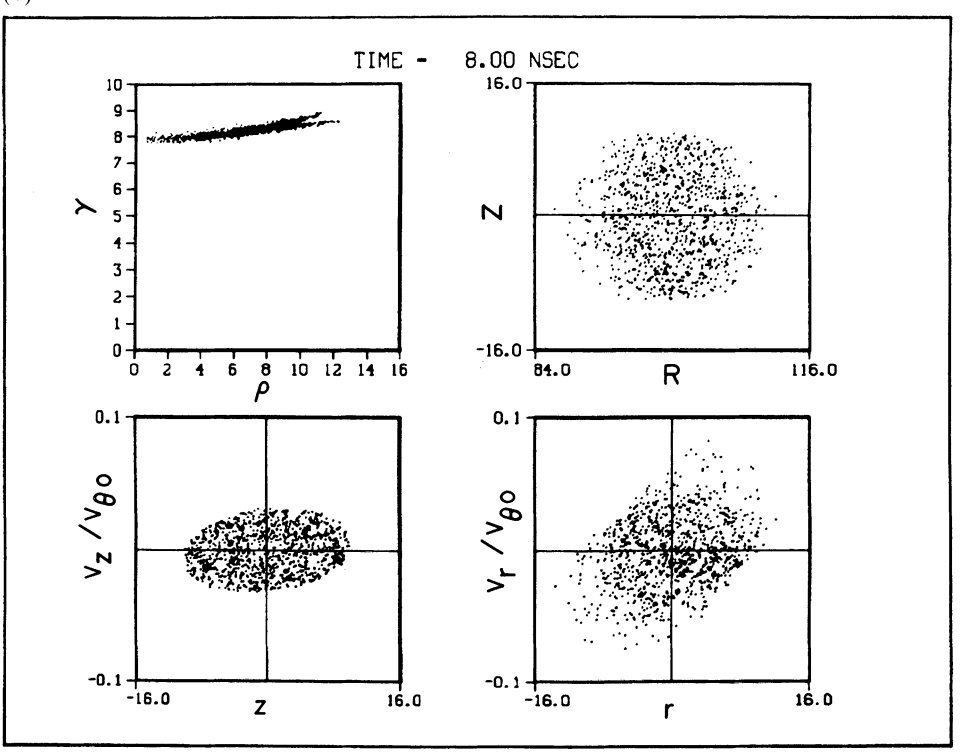
TIME - 8.00 NSEC
γ
ρ
Z
R
$v_z / v_{\theta o}$
z
$v_r / v_{\theta o}$
r

(c)

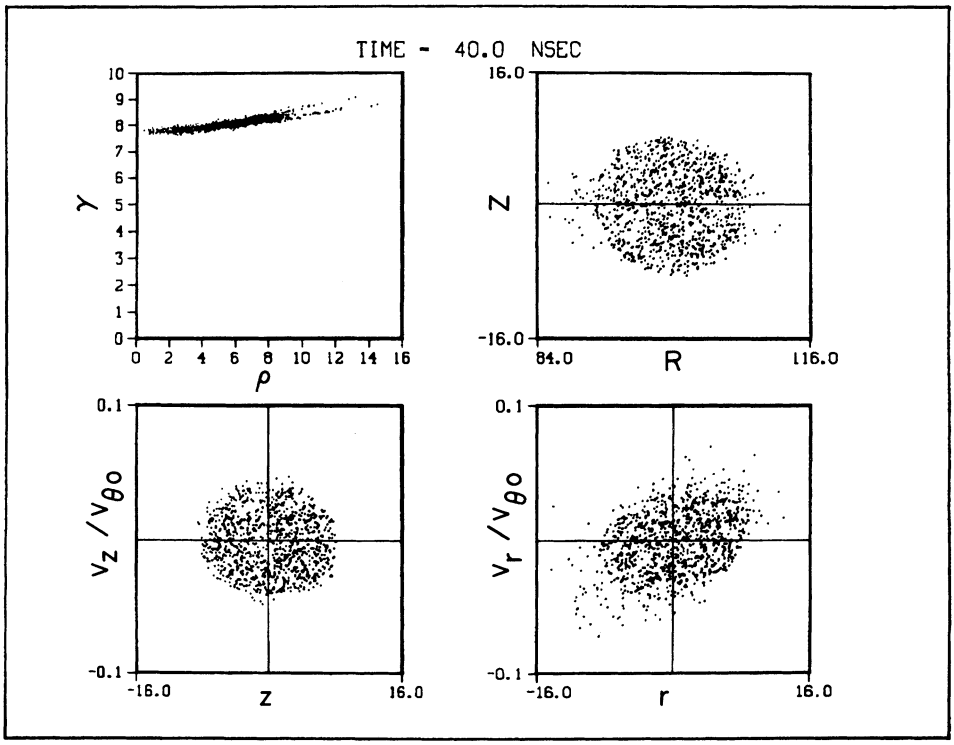

(d)

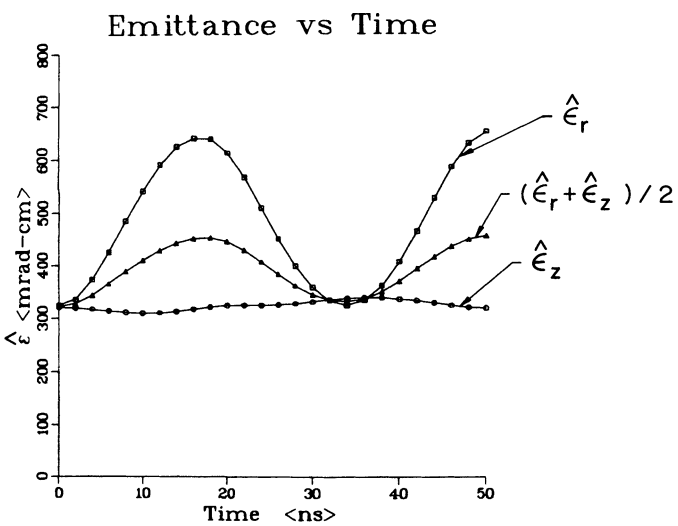

FIGURE 6 Radial profile of γ, configuration space and phase space at $t = 0$ (a); $t = 8$ (b); and $t = 40$ nsec (c), for a half-width axial energy spread of 1%. The variation of the r.m.s. emittance is shown in (d). The various parameters for this run are listed in Table III.

TABLE III
Conventional Betatron

Run. No. CONVBETA 04
Initial Beam Energy $\gamma_0 = 7.85$ (3.5 MeV)
Beam Current I (KA) = 10
Major Radius r_0 (cm) = 100
Initial Beam minor radius r_b (cm) = 8
Torus minor radius a (cm) = 16
Initial beam center position r_i (cm) = 100
Betatron Magn. Field at r_0, $z = 0$, B_{0z} (G) = 153.7
Initial emittance ϵ (rad − cm) = 0.320 (unnormalized)
Initial temperature spread (half width) $\Delta\gamma/\gamma_0 = 1\%$
External-field index $n = 0.45$
Self-field index $n_s = 0.289$

amplitude that is about 700 mrad-cm, which is slightly higher than the first peak of Fig. 6d.

The oscillations of $\hat{\epsilon}_r$ are reduced practically to zero when $\delta = 0$. This is shown in Fig. 7a. With the exception of parallel thermal energy spread, the parameters of this run are identical to those of the previous run and are listed in Table IV. In these runs, it is important to avoid introducing an artificial energy spread as, for example, by using, at $t = 0$, a cylindrical KV distribution to load the electrons in the code. In such a case, the electrons quickly acquire an "energy spread" during the run. This "thermalization" is due to the fact that a cylindrical KV distribution is not suitable for high-current electron rings that have large aspect ratio r_b/r_0, as may be seen as follows: For a uniform-density ring that is located inside a conducting torus with its minor axis lying along the minor axis of the torus, the difference in the potential energy between the outer and inner edge of a ring, along the midplane ($z = 0$), is given by

$$\Delta\Phi = \frac{-|e|}{mc^2}[\Phi_{\text{out}} - \Phi_{\text{in}}] = 2\nu(r_b/r_0)\left[\frac{1}{4} - \ln\frac{a}{r_b} - \frac{r_b^2}{4a^2}\right]. \tag{21}$$

For $a/r_b = 2$, $r_b/r_0 = 0.008$, $\nu = 0.5$, Eq. (21) gives $\Delta\Phi = -4\%$. Of course for a cylindrical KV distribution, $\Delta\Phi = 0$. Thus, a ring that has been incorrectly loaded tries to attain a more physical distribution, but in the absence of dissipation this can be achieved only temporarily. In the process, a spread in γ is developed, which is equivalent to temperature.

Often, the electron ring develops transverse oscillations. These oscillations generate a toroidal electric field that modifies the kinetic energy of the gyrating electrons according to the equation

$$mc^2\frac{d\gamma}{dt} = -|e|\,\mathbf{V}\cdot\mathbf{E} \simeq |e|(v_\theta/c)\left(\frac{\partial A_\theta}{\partial t}\right). \tag{22}$$

The change in γ can be obtained by integrating Eq. (22). Assuming that the beam is located at the center of the torus, A_θ is given by

$$A_\theta = (2I/c)\left[\frac{1}{2} + \ln(a/r_b)\right]. \tag{23}$$

(a)

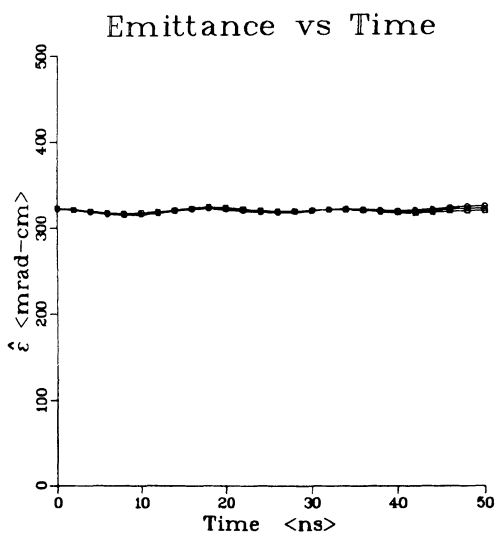

(b)

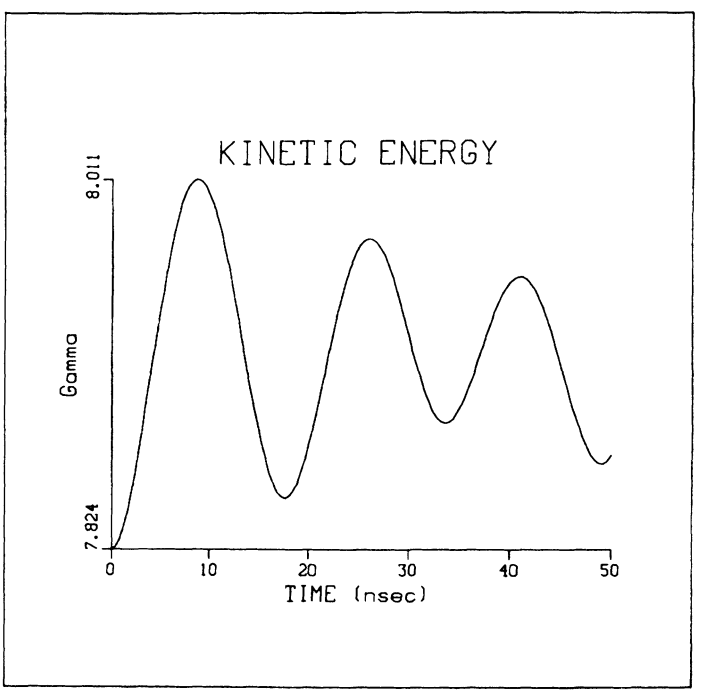

FIGURE 7 (a) Variation of the r.m.s. emittance $\hat{\epsilon}_r$, $\hat{\epsilon}_z$ and $(\hat{\epsilon}_r + \hat{\epsilon}_z)/2$ for zero energy spread; (b) temporal variation of γ. The various parameters for this run are listed in Table IV.

TABLE IV
Conventional Betatron

Run No. CONVBETA 05
Initial Beam Energy $\gamma_0 = 7.85$ (3.5 MeV)
Beam Current I (KA) = 10
Major Radius r_0 (cm) = 100
Initial Beam minor radius r_b (cm) = 8
Torus minor radius a (cm) = 16
Initial beam center position r_i (cm) = 100
Betatron Magn. Field at $r_0, z = 0$, B_{0z} (G) = 153.7
Initial emittance ϵ (rad − cm) = 0.320
Initial temperature spread (full width) $\Delta\gamma/\gamma_0 = 0.0$
External-field index $n = 0.45$
Self-field index $n_s = 0.289$

For $\gamma^2 \gg 1$ the result is

$$\gamma_f - \gamma_{\text{in}} = 2\nu \ln\left(\frac{r_{bf}}{r_{\text{bin}}}\right), \tag{24}$$

where γ_f, γ_{in} are the final and initial values of γ and r_{bf}, r_{bin} are the final and initial values of the ring radius. The variation of γ as a function of time for the run of Table IV is shown in Fig. 7b. Equation (24) predicts $\gamma_f - \gamma_{\text{in}} \simeq 0.2$, which is in good agreement with the numerical results.

Combining Eqs. (17), (19) and (20) and assuming that $n_s \ll 1/2$ and $n = 1/2$, we obtain the maximum emittance that is allowed in a betatron of major radius r_0. It is

$$\epsilon_b^2 \leqslant \frac{1}{2}\left(\frac{r_b^4}{r_0^2}\right).$$

The maximum emittance that can be accommodated in a emittance-dominated beam confined in a modified betatron is considerably greater and is given by

$$\epsilon_{mb}^2 \leqslant (r_b^4/r_0^2)(B_{0\theta}/2B_{0z})^2.$$

The ratio of the two emittances is $\epsilon_{mb}/\epsilon_b = B_{0\theta}/\sqrt{2}B_{0z}$; in general it is much greater than unity.

C. *Toroidal Corrections*[8,12,14]

The cause of these effects is the finite curvature of the electron beam orbit. For relatively large aspect ratio $r_0/r_b \gg 1$ beams, the toroidal effects become important when ν/γ_0 exceeds a few percent. The toroidal corrections have been discussed extensively in relation to the modified betatron. The fields at the center of a uniform charge and current density electron ring inside a perfectly conducting toroidal chamber of circular cross section are

$$\mathbf{E}_{\text{ind}} = -2\pi|e|n_0 r_0\left[\left(\frac{r_b^2}{a^2}\frac{\Delta r}{r_0} + \frac{1}{2}\frac{r_b^2}{r_0^2}\ln\frac{a}{r_b}\right)\hat{e}_r + \frac{r_b^2}{a^2}\frac{\Delta z}{r_0}\hat{e}_z\right], \tag{25}$$

and

$$\mathbf{B}_{\text{ind}} = -2\pi|e|n_0\beta_0 r_0\left[\frac{r_b^2}{a^2}\frac{\Delta z}{r_0}\hat{e}_r - \left(\frac{r_b^2}{a^2}\frac{\Delta r}{r_0} - \frac{r_b^2}{2r_0^2}\left\{1 + \ln\frac{a}{r_b}\right\}\right)\hat{e}_z\right], \quad (26)$$

where n_0 is the ambient density, $\beta_0 = v_{\theta 0}/c$, $v_{\theta 0}$ is the azimuthal velocity defined by

$$v_{\theta 0} = \frac{r_0\Omega_{0z}/\gamma_0}{1 + 2(\nu/\gamma_0)(1/2 + \ln a/r_b)}, \quad (27)$$

and the displacements $\Delta r, \Delta z$ of the ring from the center of the torus have been assumed to be much less than a.

Using the fields of Eqs. (21) and (22), it can be shown that the motion of the center of the beam is described by the equations

$$\Delta\ddot{r} + \omega_r^2\,\Delta r = \frac{c^2}{r_0}\frac{\delta\gamma_0}{\gamma_0}, \quad (28)$$

and

$$\Delta\ddot{z} + \omega_z^2\,\Delta z = 0, \quad (29)$$

where

$$\omega_r^2 = (\Omega_{0z}/\gamma_0)^2[\xi^2 - n\xi - 2\nu c^2/\gamma_0^3 a^2(\Omega_{0z}/\gamma_0)^2], \quad (30)$$

$$\omega_z^2 = (\Omega_{0z}/\gamma_0)^2[n\xi - 2\nu c^2/\gamma_0^3 a^2(\Omega_{0z}/\gamma_0)^2], \quad (31)$$

and

$$\xi = \{1 + (2\nu/\gamma_0)[0.5 + \ln(a/r_b)]\}^{-1}.$$

According to Eqs. (24) and (26), the equilibrium position of the orbit is displaced from the center of the minor cross section of the torus whenever the energy mismatch $\delta\gamma_0$ is not zero. The displacement is

$$\frac{\Delta r_0}{r_0} = \frac{c^2(\delta\gamma_0/\gamma_0)}{r_0^2\omega_r^2} = \frac{\gamma_0\delta\gamma_0/(\gamma_0^2 - 1)}{[1 - n/\xi - 2\nu r_0^2/\gamma_0 a^2(\gamma_0^2 - 1)]}.$$

The above equation predicts that for $\delta\gamma_0/\gamma_0 = 1\%$, $\gamma_0 = 5$, $r_0/a = 7$, $n = 1/2$, $\nu/\gamma_0 = 0.059$, i.e., for $I = 5$ kA, the ratio $\Delta r_0/r_0 = 0.05$, which for $r_0 = 110$ cm gives a displacement $\Delta r_0 = 5.5$ cm.

An interesting manifestation of toroidal effects is in the value of betatron magnetic field required to confine the rotating beam at a specific radius. When the axis of the beam lies along the axis of the torus, i.e., when $\Delta r = \Delta z = 0$, it can be shown from Eqs. (25) and (26) that the external magnetic field required for the beam to circulate at a radius r_0 is

$$B_{0z} = B_0\{1 + 2\nu/\gamma_0(0.5 + \ln a/r_b)\}, \quad (32)$$

where B_0 is the magnetic field necessary for a single particle of the same kinetic energy to circulate with radius r_0.

For the run of Table IV, the single-particle magnetic field is 134G, about 20G lower than that used in the simulation. Equation (32) predicts that the required field B_{0z} is 157.8G, approximately 4G higher than that of Table IV. The difference is related to the fact that Eq. (32) was derived under the assumption that the ratio $r_b/a \ll 1$, which is not satisfied.

III. SELF MAGNETIC-FIELD DIFFUSION

To allow the external accelerating magnetic field to penetrate inside the torus, the vacuum chamber is constructed of materials with finite conductivity. As a result, the self magnetic field diffuses out the chamber for times comparable with the magnetic diffusion time t_D. The inductive electric field generated by the changing flux acts to slow down the beam. In addition, the hoop forces increase and the induced magnetic-field components (image fields) go to zero at the end of the diffusion. However, the induced electric field components (image fields) remain the same. Although these two effects change the equilibrium position of the beam in the opposite direction, in general they do not balance each other and thus the equilibrium can be lost. This difficulty can be avoiding by compensating for the diffusion of the field with external circuits.

However, it is very unlikely that the compensation can be perfect. Therefore, in practical situations it is desirable to know the maximum permissible error in the compensation that will not result in loss of the equilibrium.

Consider an electron ring, which for $t \ll t_D$ is inside a finite-conductivity toroidal chamber with its minor axis lying along the minor axis of torus, as shown in Fig. 8. Initially, the magnetic boundary coincides with the electric boundary and has radius a. As a result of the incomplete compensation, the magnetic boundary moves, at $t \sim t_D$ to a new radius a', but the electric boundary remains at its initial position. The reduction in γ associated with the shift of the magnetic boundary can be computed from Eq. (22) and is given by

$$\Delta\gamma = -2\nu\beta_0^2 \ln\left(\frac{a'}{a}\right). \tag{33}$$

In addition to the reduction of γ, the hoop forces will increase and therefore the equilibrium position of the ring will move a distance $\Delta\hat{r}$ from the center of the torus, which was the initial equilibrium position. This distance can be computed from the radial balance equation using the fields of Eqs. (25) and (26) and the reduction of γ given by Eq. (33). The result is

$$\frac{\Delta\hat{r}}{r_0} = \frac{\nu/\gamma \ln(a'/a)}{[1 - n - (n_s r_b^2/a^2)(1 + 2\gamma^2\,\delta a/a)]},$$

where $\delta a = a' - a$.

In order to keep the displacement $\Delta\hat{r} \ll a$, it is necessary to avoid the singularity of the denominator, i.e.,

$$(n_s r_b^2/a^2)(1 + 2\gamma^2\,\delta a/a) \ll 1 - n.$$

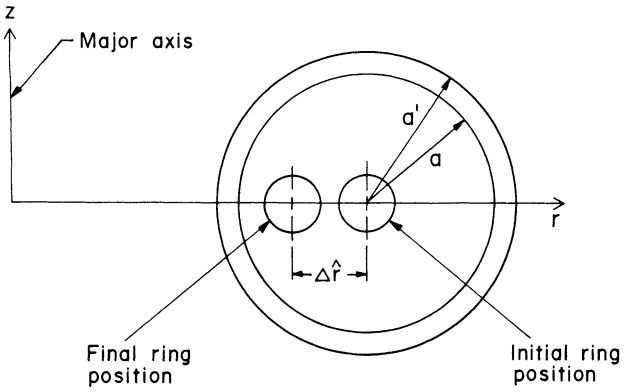

FIGURE 8 Initial and final ring position resulting from the incomplete compensation of wall currents during diffusion of self-magnetic field.

For $\delta a/a = 10\%$, $\gamma = 7$, $n = n_s \approx 1/2$, the above relation gives

$$\left(\frac{r_b}{a}\right)^2 \ll \frac{1}{11}.$$

The corresponding displacement of the equilibrium position for $a = 15$ cm, $r_0 = 100$ cm and $\nu = 0.59$ is 1.6 cm. Therefore, the shift in the equilibrium position during diffusion is manageable, provided that the compensation is better than 90%.

IV. CONCLUSIONS

The main conclusions that may be drawn from the present studies are: Like the modified betatron, the conventional betatron is sensitive to the energy mismatch and the diffusion of the self magnetic field. However, in contrast to the modified betatron, the conventional betatron cannot accommodate large thermal energy spread and large emittance. These advantages of the modified betatron, together with its superior stability[22–24] properties make it a more appropriate accelerator when intense beams are desired.

Finally, it is necessary to keep the ratio $r_{b/a} \ll 1$, in both devices, in particular in the high-current regime.

REFERENCES

1. T. J. Fessenden et al., Proc. of the Intern. Top. Conf. on High-Power Electron and Ion Beam Research and Technology, Palaiseau, France, June 29–July 3, 1981, p. 813.
2. R. Briggs, *IEEE Trans. Nucl. Sci.*, **NS-28**, 3360 (1981).
3. A. I. Paulovskii et al., *Sov. Phys. Tech. Phys.*, **22**, 218 (1977).
4. A. G. Bonch-Osmolovskii, G. V. Dolbilow, I. N. Ivanov, E. A. Perelshtein, V. P. Sarantsev, and O. I. Yarkovoy, JINR-Report P9-4135, Dubna, 1968.
5. P. Sprangle and C. A. Kapetanakos, *J. Appl. Phys.*, **49**, 1 (1978).
6. N. Rostoker, *Comments on Plasma Physics* (Gordon and Breach Science Publ. Inc., 1980) Vol. 6, p. 91.

7. C. L. Olson and V. Schumacher, *Collective Ion Acceleration* (Springer-Verlag, Berlin, Heidelberg, New York, 1979), p. 199.
8. P. Sprangle, C. A. Kapetanakos, and S. J. Marsh, Proc. of the Intern. Top. Conf. on High-Power Electron and Ion Beam Research and Technology, Palaiseau, France, June 29–July 3, 1981, p. 803; also NRL Memo Report 4666 (1981).
9. G. Barak, D. Chernin, A. Fisher, H. Ishizuda, and N. Rostoker, Proc. of the Intern. Top. Conf. on High Power Electron and Ion Beam Research and Technology, Palaiseau, France, June 29–July 3, 1981, p. 795.
10. H. S. Uhm and R. C. Davison, MIT, Plasma Fusion Center Report No. JA-81-30, 1981.
11. C. A. Kapetanakos, P. Sprangle, and S. J. Marsh, NRL Memo Report 4835, 1982; also *Phys. Rev. Lett.*, **49**, 741 (1982).
12. C. A. Kapetanakos, P. Sprangle, D. P. Chernin, S. J. Marsh, and I. Haber, NRL Memo Report 4905, 1982; also *Phys. of Fluids* (1983).
13. W. M. Manheimer and J. M. Finn, *Particle Accelerators*, 1983.
14. D. P. Chernin and P. Sprangle, *Particle Accelerators*, **12**, 85 (1982).
15. G. Barak and N. Rostoker, *Phys. of Fluids*, **26**, 3 (1983).
16. D. Taggart, M. Parker, H. J. Hopman, and H. H. Fleischmann, *IEEE Trans. Nucl. Sci.*, **30**, 3165 (1983); this reference describes a plasma betatron, in which the electron ring is neutralized.
17. C. Roberson, A. Mondelli, and D. Chernin, *Phys. Rev. Lett.*, **50**, 507 (1983).
18. D. W. Kerst, *Nature*, **157**, 90 (1940).
19. D. W. Kerst et al., *Rev. Sci. Instrum.*, **21**, 462 (1950).
20. J. Lawson, *The Physics of Charged-Particle Beams* (Clarendon Press-Oxford, 1977), p. 189.
21. J. M. Peterson, LBL Report 15206 (1982).
22. P. Sprangle and J. Vomvoridis, NRL Memo Report 4688, 1981.
23. T. P. Hughes and B. B. Godfrey, Mission Research Corp. Report No. AMRC-R 354, 1982; also AMRC-R-332, 1982.
24. P. Sprangle and D. Chernin, NRL Memo Report 5176, 1983.

APPENDIX A

Consider a straight electron beam of radius r_b inside a cylindrical, conducting pipe of radius a as shown in Fig. 5. The total vector potential $\mathbf{A_T} = \mathbf{A_p} + \mathbf{A_h}$, where $\mathbf{A_p}$ is the particular and $\mathbf{A_h}$ is the homogeneous solution of the wave equation.

When the displacement current is neglected, the particular solution for $\rho \geqslant r_b$ is

$$\mathbf{A_p}(\mathbf{p}, \phi, t) = -\frac{2I(t)}{c} \ln |\mathbf{p} - \Delta(t)| \hat{e}_\theta, \tag{A-1}$$

where

$$|\mathbf{p} - \Delta(t)| = [p^2 + \Delta^2(t) - 2p\Delta(t) \cos(\phi - \alpha(t))]^{1/2}$$

and $I(t) = -|e|n_0 v_{\theta 0} n r_b^2$ is the beam current.

Similarly, the homogeneous solution is

$$\mathbf{A_h}(p, \theta, t) = \sum_{l=0}^{\infty} a_l(t)(p/a)^l e^{il\phi} \hat{e}_\theta + c \cdot c., \tag{A-2}$$

where the coefficients are to be determined from the boundary conditions. For a perfect conductor, $A_T = 0$ at $p = a$ and Eqs. (A-1) and (A-2) give

$$a_0 = (I/c) \ln a$$

$$a_l = -(I/c) l^{-1} (\Delta/a)^l e^{-il\alpha}, \; l = 1, 2, \ldots$$

The magnetic field at the center of the beam is

$$B_\phi(\Delta, \alpha) = -\frac{\partial A_h}{\partial p} = -\frac{2I}{ac}\sum_{l=1}^{\infty}\left(\frac{\Delta}{a}\right)^{2l-1}$$

$$= -\frac{2I}{a^2 c}\frac{\Delta}{(1 - \Delta^2/a^2)}. \tag{A-3}$$

Equation (A-3) was derived without any assumption about the beam radius.